Transfer path analysis and its application in low-frequency vibration reduction of steering wheel of a passenger vehicle

Shaogan Ye [a], Liang Hou [a,*], Pandeng Zhang [b], Xiangjian Bu [a], Jiawei Xiang [c], Hesheng Tang [c], Jiahe Lin [a]

[a] Department of Mechanical and Electrical Engineering, Xiamen University, Xiamen 361102, China
[b] King Long Automotive Engineering Research Institute, Xiamen 361023, China
[c] School of Mechanical and Electrical Engineering, Wenzhou University, Wenzhou 325035, China

ARTICLE INFO

ABSTRACT

The demands on improving the noise, vibration and harshness of passenger vehicles are growing rapidly. Low-frequency vibration of steering wheel is one of the most important factors leading to the discomfort of drivers. This study proposes a systematic analysis methodology to reduce the low-frequency vibration of steering wheel using classical transfer path analysis (CTPA). The theoretical basics of TPA using dynamic stiffness approach and inverse matrix approach are briefly introduced, and then the experimental apparatus and analysis procedures in performing the TPA are introduced. The static forces in the rubber mounts of the powertrain system are calculated, the dynamic stiffness of the rubber mounts are estimated, and the operational forces are determined. The contributions of different transfer paths to the vibration of steering wheel are analyzed and compared, and the predominant causes are identified. The results show that the vibration of steering wheel along the X direction is protruded at the engine ignition frequency, and the vibration of the exhaust system along the X direction contributes most to the vibration because of large frequency response function. The mounting structure of the exhaust system is modified based on modal analysis results using finite element method to reduce the vibration of steering wheel.

© 2019 Elsevier Ltd. All rights reserved.

1. Introduction

The noise, vibration and harshness (NVH) are becoming one of the most important performance indexes in the automobiles [1,2], high-speed trains [3,4], passenger vehicles and many industrial areas [5–8]. Great attentions have been paid to increase the comfort of passengers, drivers and machine operators. Due to the fact that the drivers have a longer time exposing to the vibrating environment than the passengers, the demand on improving the comfort of drivers in passenger vehicles are increasing more rapidly [9]. There are mainly three aspects that affecting the comfort of drivers in passenger vehicles. The first one is the perceived noise in the ear, the second one is the vibration of the seat, and the last one is the vibration of the steering wheel. The perceived sound in passenger vehicles can be improved by using sound-absorbing materials in recent years, while the vibration of seat and steering wheel cannot be easily solved and remains a challenging task for most of the manufactures of passenger vehicles.

Many efforts have been carried out in order to solve the NVH problems and improve the NVH performance of complex mechanical products. Transfer path analysis (TPA) method is considered to be an effective method in identifying the dominant sources. Based on the TPA, the root causes of noise and vibration problems can be detected accurately, the performance targets for the key components can be set reasonably, and the design improvements can be evaluated quickly. Classical TPA (CTPA) is often employed in engineering practice. Two steps are required to establish the CTPA model. The first step is to estimate the decoupled frequency response functions (FRFs), and the second step is to identify the operational forces. The FRFs are obtained from experimental measurements using a shaker or impact hammer for the structural forces using reciprocity techniques. The operational forces are identified by performing several measurements at different operational conditions. The responses at the receiver points are then estimated by calculations, and the contribution of each transfer path can be determined by a combination of the measured FRFs and the corresponding operational forces.

* Corresponding author.
    E-mail addresses: shaoganye@xmu.edu.cn (S. Ye), hliang@xmu.edu.cn (L. Hou), zhangpd@mail.king-long.com.cn (P. Zhang), bxj@xmu.edu.cn (X. Bu), jwxiang@wzu.edu.cn (J. Xiang).

Nomenclature

a_0	the reference acceleration, $a_0 = 1\ \text{m/s}^2$
$a_1, a_2, a_3, a_4, a_5, a_6$	the coefficients
$a(j\omega)$	the acceleration
$a_i(j\omega)$	the vibration acceleration at the source point i
$a_k(j\omega)$	the vibration acceleration at the receiver point k
$k_i(j\omega)$	the dynamic stiffness
$y_{ik}(j\omega)$	the response at the receiver point k under the effects of source point i
$y_k(j\omega)$	the total response at the receiver point k
$H_{ik}(j\omega)$	the FRF between the uncoupled source point i and the receiver point k
L_a	the acceleration level
L_{FRF}	the FRF level
L_N	the force level
F	the static force acting on the rubber mounts
F_e	the shear force
$F_i(j\omega)$	the force at the source point i
F_N	the normal force acting on each front rubber mount
F_0	the reference force, $F_0 = 1\ \text{N}$
F_f	the compression force
FRF_0	the reference FRF, $FRF_0 = 1\ (\text{m/s}^2)/\text{N}$
$FRF(j\omega)$	the FRF
$\boldsymbol{A}(j\omega)$	the vector of the responses in the passive part
$\boldsymbol{F}(j\omega)$	the vector of the operational forces
$\boldsymbol{H}(j\omega)$	the impedance matrix between the active and passive parts
α	the angle between the lines $O_{FL}O_{FR}$ and $O_{FL}B$ (or $O_{FR}B$)
β	the mounting angle of the rubber mounts (defined by the angle between the lines $O_{FL}O_{FR}$ and $O_{FL}A$ (or $O_{FR}A$))

In the CTPA, there are mainly two drawbacks. The first drawback is that the CTPA takes too much time, and the second drawback is that there are some difficulties in determining the operational forces. In performing CTPA, the active part generating the vibration should be removed in the measurements of FRFs. This action might add to the time and bring some errors. In order to improve the performance of CTPA methods, several advanced TPA methods have been developed, including the Component-based TPA [10], Operational TPA (OPA) [11], OPAX [12], and Global Transfer Direct Transfer (GTDT) methods [13]. The OPAX method is developed based on the theory frame of the CTPA. In OPAX method, the operational forces are identified in a parametric way from the operational data. A balance between the accuracy and measurement time are considered to be obtained using the OPAX method. However, the system should still be disassembled for measurements of FRFs.

In order to overcome the drawbacks regarding the time-consumption in disassembling the systems and the changes in the boundary conditions, an alternative method is developed for the In-Situ estimation of the FRFs. This method uses the measured operational data with a known external force. Quite a good combination of the accuracy and efficiency can be obtained using the method because the system does not need to be disassembled. However, it is difficult and even impossible to be employed in practical complex mechanical systems due to two difficulties. The first difficulty is that the forces acting on the passive parts should be known, and the second difficulty is the large number of uncorrelated forces acting on the active part under actual operating conditions.

The In-Situ blocked force TPA (BF-TPA) is introduced recently. Using this method, the blocked forces of the system at the contact points of the system and the subsystems should be measured. No specific requirements are needed for the BF-TPA method, which is its main advantage. Because the blocked forces of the main system do not dependent on the condition of the subsystem, the method does not require the disconnections of the active and passive systems.

In-Situ BF-TPA was used to analyze the beam-like sources and receivers to solve the difficulties encountered using CTPA [14]. The transfer path of road noise and the contributions of the mounts of the suspension system to the road noise were identified using the method [15]. The transfer path of the steering system and other major sources of interior noise in the power steering system were also identified using the method. The effectiveness of BF-TPA in several different boundary conditions was validated, and the blocked force on the suspension system of an electric vehicle was identified [16]. A comparison of the effectiveness of CTPA, OPA, and In-Situ BF-TPA methods was studied for an electric vehicle [17]. The structure-borne path of rumbling noise in a vehicle cabin was identified using the CTPA and BF-TPA methods, and the differences between CTPA and BF-TPA were compared. The roll bar was modified by adding mass to change its structural dynamics near the engine mounts to increase the sound quality of rumbling noise at shaft rotational speeds lower than 3500 r/min [18].

However, the coherence is small at low frequencies (smaller than 100 Hz) using the In-Situ BF-TPA, which might result in inaccurate estimated blocked forces and vibration velocities at frequencies under 100 Hz due to small coherence [18]. This indicates that the In-Situ BF-TPA might not be efficient in low frequency range, which is quite important in the evaluation of the performance of passenger vehicles. In addition, the uses of other advanced TPA methods remain challenging in solving the NVH problems in engineering practice. Therefore, the CTPA remains to be the good choice in solving the NVH problem of passenger vehicles under low frequency range.

The aim of this study is to propose a systematic analysis methodology to reduce the vibration of steering wheel of a passenger vehicle using CTPA methods under low frequency range (0–100 Hz). The remainder of this study is organized as follows. The theoretical basics of the CTPA using the dynamic stiffness and inverse matrix approach based methods are briefly introduced in Section 2. In Section 3, the experimental setups in measuring the vibration of the steering wheel, the dynamic stiffness of the rubber mounts, and the FRFs are introduced. The experimental results are presented concerning the measured vibrations of the steering wheel, contributions of different transfer paths, and comparisons of the operational forces and FRFs. The modifications of the mounting structure based on modal analysis to reduce the vibration of the steering wheel are presented in Section 4, followed by the conclusions given in Section 5.

2. Theoretical basics

In CTPA, the operational forces should be determined first. Three methods are considered to be valid in identifying the operational forces. The first method is to measure the operational forces directly, which is often difficult or impossible to be implemented due to the limitations of the space and support surfaces. The second method is to calculate the operational forces by a combination of the operational accelerations of the contacting points with the corresponding acceleration matrix. This method is a bit

time-consumption due to the requirements of large number of measurements. The third method is to calculate the operational forces using the relative displacement and dynamic stiffness of the mount. The method requires that the dynamic stiffness of the mount should be known, which is often available for vehicle manufacturers. Due to these reasons, a combination of the second and third methods are used here, which are both based on the source-path-receiver model. In order to distinguish the method with the inverse matrix method (the operational forces will be calculated with this method for comparisons), the method will be denoted as the combined method in this study as presented in the following section. The theoretical basics of these two methods are to be briefly described in the following sections.

2.1. Theory of dynamic stiffness approach based transfer path analysis

In the dynamic stiffness approach based TPA method, the global system is divided into the active part and the passive part. The active part is the source points, and the passive part is the receiver points. A transfer path is then defined for each degree of freedom (DOF) acting at the contacting points between the active part and the passive part. For structural vibrations, the energy generated by the structural forces of the active part transmits through mount connections to the receiver points of the passive part. The responses at the receiver point can be calculated by summing all the contributions generated by each path, as described by:

$$y_k(j\omega) = \sum_{i=1}^{M} y_{ik}(j\omega),\tag{1}$$

where $y_k(j\omega)$ is the total response at the receiver point k, and $y_{ik}(j\omega)$ is the response at the receiver point k under the effects of interacting point i, as given by:

$$y_{ik}(j\omega) = H_{ik}(j\omega)F_i(j\omega),\tag{2}$$

where $H_{ik}(j\omega)$ is the FRF between the uncoupled interacting point i and the receiver point k, $F_i(j\omega)$ is the operational force at the interacting point i, $j = \sqrt{-1}$, ω is the angular frequency, $\omega = 2\pi f$, f is the frequency of the operational force.

In order to obtain the responses at the receiver points, the FRFs between the uncoupled source points and the receiver points and the operational forces at the source points should be determined. Due to the facts that the FRFs can be measured, the remaining unknown variable is the operational forces at the source points. In the dynamic stiffness approach based method, the operational force in the source is given by:

$$F_i(j\omega) = -\frac{1}{\omega^2} K_i(j\omega)[a_i(j\omega) - a_k(j\omega)],\tag{3}$$

where $K_i(j\omega)$ is the dynamic stiffness, $a_i(j\omega)$ is the vibration acceleration at the active point i, and $a_k(j\omega)$ is the vibration acceleration at the passive point k.

2.2. Theory of inverse matrix approach based transfer path analysis

The operational forces can also be calculated using the inverse matrix approach based method, as described by:

$$F(j\omega) = H(j\omega)^{-1} A(j\omega),\tag{4}$$

where $F(j\omega)$ is the vector of the operational forces, $H(j\omega)$ is the admittance matrix from the passive points to the active points, $A(j\omega)$ is the vector of the measured vibration responses in the interacting points at the actual operating conditions, the superscript -1 represents the inverse of the admittance matrix.

The expressions of the vectors of the operational forces, the admittance matrix and the vector of the measured vibration responses are respectively described by:

$$F(j\omega) = [\ F_1(j\omega) \quad ... \quad F_m(j\omega) \quad ... \quad F_M(j\omega)\ ]^T\tag{5}$$

$$H(j\omega) = \begin{bmatrix} H_{11}(j\omega) & \cdots & H_{1n}(j\omega) & \cdots & H_{1N}j(\omega) \\ \vdots & \vdots & \vdots & \vdots & \vdots \\ H_{m1}(j\omega) & \cdots & H_{mn}(j\omega) & \cdots & H_{mN}(j\omega) \\ \vdots & \vdots & \vdots & \vdots & \vdots \\ H_{M1}(j\omega) & \cdots & H_{Mn}(j\omega) & \cdots & H_{MN}(j\omega) \end{bmatrix}\tag{6}$$

$$A(j\omega) = [\ a_1(j\omega) \quad ... \quad a_n(j\omega) \quad ... \quad a_N(j\omega)\ ]^T\tag{7}$$

where M is the total number of sources in the active parts, N is the total number of responses in the passive parts, m is the mth source, and n is the nth response. Often, N should be no less than M.

2.3. Analysis procedures

According to the theory of the dynamic stiffness approach based and inverse matrix approach based TPA, the analysis procedures are often divided into four steps. First, the source-path-response model is constructed by defining the sources, transfer paths and receivers clearly. Second, the experimental tests are performed to measure the vibration accelerations to calculate the FRFs. Third, the dynamic stiffness and the impedance matrix should be calculated to determine the operational forces. Last, the responses are calculated and the contributions of different sources are determined.

3. Experiments and analyses

The layout of the passenger vehicle is shown in Fig. 1. For the investigated mid-size passenger vehicle, an inline internal combustion four-cylinder four stroke engine was used. The engine is supported by four rubber mounts. For the passenger vehicle, the global coordinate system OXYZ was defined. The origin O was located in the center of gravity of the passenger vehicle, the X and Y axes are in parallel to the horizontal plane, and the Z axis is normal to the horizontal plane with its positive direction upward. The positive direction of the X axis points to the front of the passenger vehicle, and the positive direction of the Y axis points to the left of the passenger vehicle. In this study, two identical flat rubber mounts were used in the front left and right powertrain systems, and two identical V-shape rubber mounts were
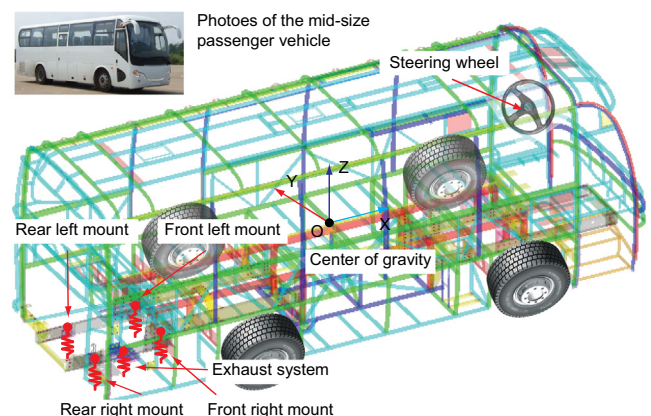

Fig. 1. Layout of the mid-size passenger vehicle.

used in the rear left and right powertrain systems. The four rubber mounts were denoted by FLM (front left mount), FRM (front right mount), RLM (rear left mount) and RRM (rear right mount), respectively. The engine forces are transferred to the rubber mounts of the powertrain through different transfer paths, including the main bearings, cylinder block, crankshaft train and housing. The exhaust system (denoted by EXS) is supported by two hooks and one vibration isolator. The exhaust system also generates forces, and then transmitted to the body of the passenger vehicle. The passenger vehicle vibrates as its body is excited by these forces transmitted from the rubber mounts and the exhaust system. The multi-spring suspension system is used to reduce the vibration generated from the road and tires. The rated allowable number of passengers are 33. The length, width and height of the passenger vehicle are 8.245 m, 2.840 m and 3.325 m, respectively. At normal driving condition, the engine, exhaust system, road and tires are the main sources that generating the vibration, while only the engine and exhaust system produce the vibration at the idle condition.

In this study, three types of experimental tests are to be carried out, including the measurements of vibration of the steering wheel, measurements of the dynamic stiffness of the rubber mounts, and measurements of the FRFs between the sources and receivers. The details of these measurements will be given in the following sections.

3.1. Vibration measurements of the steering wheel and analyses

The vibration of the steering wheel was measured at the idle condition. At the idle condition, the passenger vehicle is at a standby condition, and the tires and transmission devices are kept unmovable. The rotational speed of the engine was around 660 r/min. In order to measure the vibration of the steering wheel, one tri-axial accelerometer (Type 356B10, PCB) was attached to the top of the steering column. The vibration at this point is considered to be meaningful in reflecting the vibration characteristics of the steering wheel in engineering practice. The signal was acquired using the multi-channel signal acquisition device (LMS SCADAS Mobile), and analyzed in a personnel computer (Lenovo G510). The frequency range is 0–256 Hz, and the sampling frequency is 1 Hz, which is enough to give a detailed analysis of the vibration accelerations in the low frequency range of 0–100 Hz. The Hanning window was employed to reduce the signal leakages. It should be noticed that these devices are also used in the measurements of operational forces and FRFs in the following sections.

In most engineering practices, the acceleration level is used to present the vibration instead of using directly the acceleration. The acceleration level is calculated by:

$$L_a = 10 \cdot \log\left[(a(j\omega)/a_0)^2\right], \tag{8}$$

where a_0 is the reference acceleration, $a_0 = 1$ m/s^2.

The measured vibration acceleration level of the steering wheel at the idle condition is shown in Fig. 2. The figure clearly shows

that there are several peaks at frequencies which are integers multiple of the engine ignition frequency. The engine ignition frequency is around 22 Hz ($f = nl/60\tau$, n is the rotational speed of the engine shaft, l is the number of cylinder, and τ is the coefficient relating to the stroke of the engine, $\tau = 2$ in this study). The figure also shows that the vibration acceleration at the frequency of around 22 Hz is dominant, which is far larger than the vibration velocities at other harmonic frequencies (44 Hz, 66 Hz and 88 Hz). In addition, at the engine ignition frequency, the vibration acceleration along the X direction is the largest, far larger than the vibration accelerations along the Y and Z directions. These results indicate that the vibration along the X direction at the engine ignition frequency might be the main cause of driver's discomfort for the passenger vehicle. Based on these measured results, it is desired to pay more attention on the vibration accelerations of the steering wheel at the engine ignition frequency, especially the one along the X direction.

3.2. Dynamic stiffness estimations

In this study, the sources include the operational forces in the four rubber mounts and the exhaust system. In theory, the operational forces include the forces and moments of force. The moments of force around the X, Y and Z directions are often considered to be small in engineering practice, and thus the moments of force are neglected in this study. There are totally 15 sources because all the operational forces with their components along the X, Y and Z directions are considered. Only one receiver is defined in the steering wheel in the driver compartment. The transfer paths are the paths from each source to the complex dynamic systems of the passenger vehicle, and there are 15 transfer paths.

The dynamic stiffness of the rubber mounts was measured using the high frequency elastomer test system (MTS Model 831.50). The dynamic stiffness was measured at a frequency range of 2–200 Hz, with several discrete static forces of 20, 100, 300, 500, 1000, 1500, 2000, 2500, 3000 and 4000 N. Because the actual force acting on the rubber mounts of the passenger vehicle in the operational condition are often not the same as in the experiments, an estimation of the dynamic stiffness is required. This is achieved by interpolating the measured dynamic stiffness using quadratic polynomial regression fitting method as given by:

$$K(j\omega) = a_1 + a_2 F + a_3 F^2 + a_4 \omega F + a_5 \omega + a_6 \omega^2, \tag{9}$$

where $K(j\omega)$ is the dynamic stiffness of the rubber, F is the static force acting on the rubber mounts.

For the two rear flat rubber mounts, the dynamic stiffness can be directly calculated using the measured data because the static forces acting on the two rubber mounts can be calculated simply. However, for the two front V-shape rubber mounts, the dynamic stiffness cannot be directly calculated using the measured data
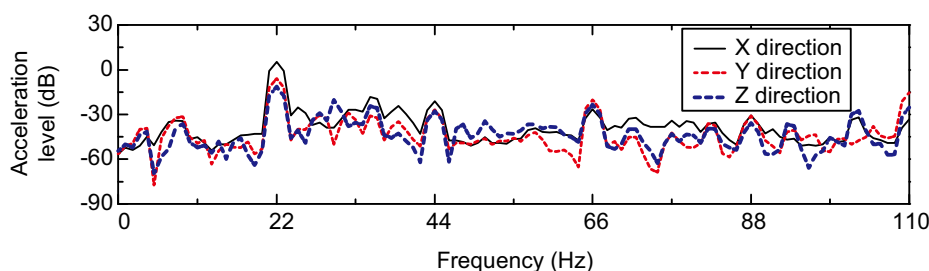

Fig. 2. Measured vibration accelerations along the X, Y and Z directions of the steering wheel at the idle condition.

because the static forces acting on the two rubber mounts cannot be simply determined.

In order to obtain the accurate dynamic stiffness, the static forces acting on the two front rubber mounts should be determined. The static forces acting on the two V-shape rubber mounts were shown in Fig. 3. Two local coordinate systems ($O_{FL}X_{FL}Y_{FL}Z_{FL}$, $O_{FR}X_{FR}Y_{FR}Z_{FR}$) were defined for each rubber mount, respectively. When there are no normal forces acting on the rubber mounts, the centerlines of the rubber mounts are $O_{FL}A$ and $O_{FR}A$, respectively. When there are normal forces acting on the rubber mounts, the centerlines of the rubber mounts are $O_{FL}B$ and $O_{FR}B$, respectively. The forces acting on each V-shape rubber mount can be divided into the shear force, F_e, and the compression force, F_f, as described by:

$$\begin{cases} F_e = \frac{F_N}{\sin\alpha}\sin(\alpha + \beta) \\ F_f = \frac{F_N}{\sin\alpha}\cos(\alpha + \beta) \end{cases}, \tag{10}$$

where F_N is the normal force acting on each front rubber mount, α is the angle between the lines $O_{FL}O_{FR}$ and $O_{FL}B$ (or $O_{FR}B$), β is the mounting angle of the rubber mounts (defined by the angle between the lines $O_{FL}O_{FR}$ and $O_{FL}A$ (or $O_{FR}A$)).

In addition, it is also necessary to transform the obtained dynamic stiffness along the local Y_{FL}, Y_{FR}, Z_{FL} and Z_{FR} directions into the global Y and Z directions as described by:

$$\begin{cases} K_y = (K_{YFL} + K_{YRL})\sin^2\theta + (K_{ZFL} + K_{ZRL})\cos^2\theta \\ K_z = (K_{YFL} + K_{YRL})\cos^2\theta + (K_{ZFL} + K_{ZRL})\sin^2\theta \end{cases}, \tag{11}$$

It should be noticed that the dynamic stiffness of the two V-shape rubber mounts along the X direction are not calculated by the above method. These values were directly obtained by the test assuming a small static force of 20 N because the static forces acting on the rubber mounts along the X direction were assumed to be small.

In addition, the exhaust system was hanged using steel wire rope, only the dynamic stiffness along the Z direction is available for the automobile manufacturer. Therefore, the dynamic stiffness approach based TPA method is not suitable for calculating the operational forces of the exhaust system. Instead, the operational forces were calculated by the using the inverse matrix approach based TPA method.

The operational forces can be estimated when the dynamic stiffness has been determined using the dynamic stiffness approach based TPA method, or when the inverse matrix has been determined using the inverse matrix approach based TPA method. In most engineering practices, the force level is used to represent the operational force instead of using directly the force. The force level is calculated by:
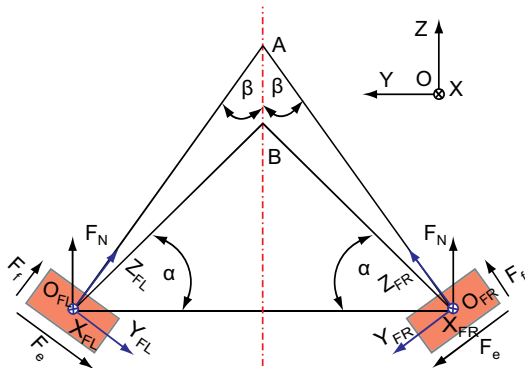
$$L_N = 10 \cdot \log\left[(F(j\omega)/F_0)^2\right], \tag{12}$$

where F_0 is the reference force, $F_0 = 1$ N.

3.3. Measurements of the admittances, accelerations and frequency response functions

Before calculating the operational forces, the admittance matrix and vibration responses are measured. For the passenger vehicle operating at the idle condition, the powertrain system and the exhaust system are the main sources in the active part, the body of the passenger vehicle is the passive part, and the receiver is the steering wheel along the X direction. The powertrain system interacts with the body with four rubber mounts. The vibration generated by the powertrain system transmits to the body through the interacting rubber mounts. Besides, the vibration generated by the exhaust system also transmits to the body by the interactions between the exhaust system and the body. Therefore, there are 15 sources and 15 transfer paths in the TPA of the passenger vehicle at the idle condition in this study as illustrated in Fig. 4. The experimental set-up was constructed as shown in Fig. 5. In order to obtain the admittance matrix, the passenger vehicle was disassembled. The engine and exhaust system were removed from the passenger vehicle. Before disassembling, the vibrations at the 5 passive points were measured at the actual operating conditions to obtain the vector of the accelerations used to calculate the operational forces in the inverse matrix method. Besides, the accelerations at the four active points and four passive points in the four rubber mounts were also measured to calculate the operational forces using the dynamic stiffness method.

Two more reference points were respectively attached to each rubber mount and the exhaust system to improve the accuracy of the calculated admittance matrix. There were four tri-axial accelerometers ((Type 356B10, PCB)) attached to each rubber mount. They are denoted by the active points, passive points and reference points. There were only three accelerometers attached to the exhaust system because no active point was defined for the exhaust system due to the fact that the operational forces of the exhaust system cannot be determined using the dynamic stiffness method. The accelerations were measured at five passive points and ten reference points when the impact hammer (Type 086C03, PCB) with a force transducer (Type 086D05, PCB) excited the four rubber mounts and the exhaust system respectively.
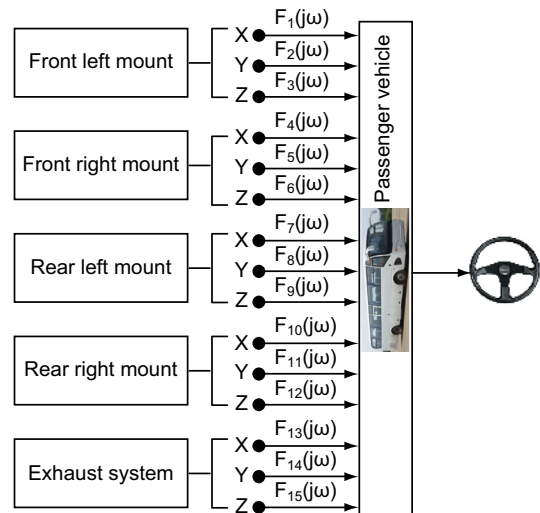

Fig. 3. Forces acting on the two V-shape rubber mounts.

Fig. 4. Schematic of the transfer path analysis of the passenger vehicle at the idle condition.
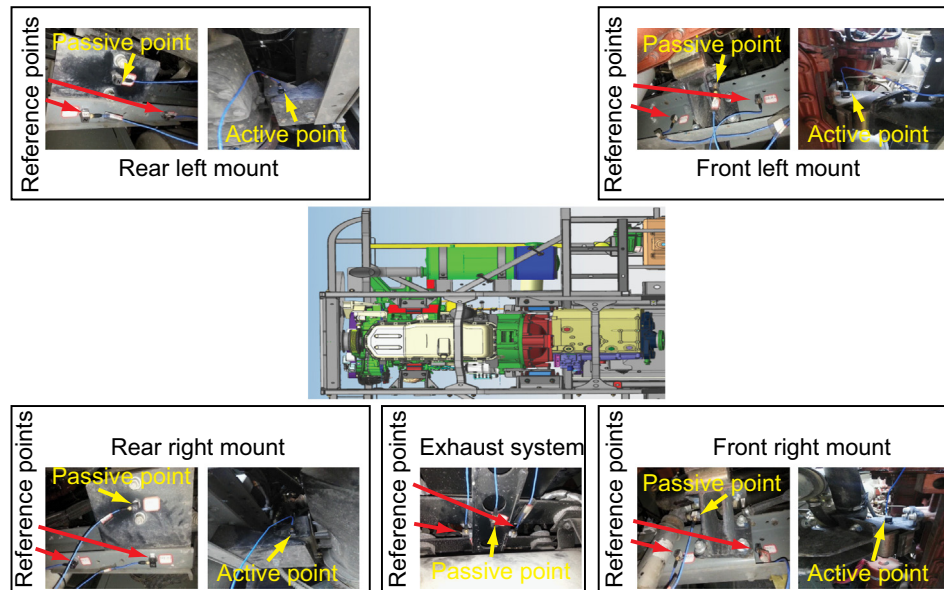
Fig. 5. Experimental set-up in the measurements of impedances, accelerations and FRFs.

In addition, the FRFs between the interacting points and the receiver point were also measured.

In the experiments, the rubber hammer was used to excite the passenger vehicle because the focus of this study is the vibration at low frequency range (0–100 Hz). Considering of the noise in the input and output signals, the Hv-estimation method is employed. The method is suitable to be used to handle the noise, and thus the accuracy of the obtained FRFs can be improved. The hitting process was repeated six times at one measuring point. The coherences between the tests were all bigger than 0.9. The FRFs are obtained by averaging the six measured FRFs.

Similarly, the FRF level is used to represent the FRF instead of using directly the FRF. The FRF level is calculated by:

$$L_{FRF} = 10 \cdot \log\left[(FRF(j\omega)/FRF_0)^2\right], \tag{13}$$

where FRF_0 is the reference FRF, $FRF_0 = 1$ (m/s²)/N.

3.4. Validations of the method

In order to validate the method, the calculated and measured vibration accelerations of the steering wheel along the X direction were compared as shown in Fig. 6. It is seen that the calculated vibration accelerations are larger than the measured ones at most of the frequencies, and the vibration accelerations calculated with the inverse matrix method are larger than the vibration accelerations calculated with the combined method. The errors between

the calculated and measured vibration accelerations are mainly caused by the changes in the dynamic stiffness by the decoupling of the powertrain system and the body of the passenger vehicle required for the measurement of the decoupled mobility. The actual dynamic stiffness might be smaller when the engine and exhaust system are not removed from the passenger vehicle. These errors between the calculated and measured results cannot be avoided due to the limitations of the TPA in engineering practice. The differences between the two calculated results might mostly be caused by the differences in the calculated operational forces. Most of the calculated operational forces using the inverse matrix method were larger than those calculated using the combined method. In spite of these discrepancies, good agreements between the calculated and measured results can be seen. These results imply that the proposed combined method is more accurate than the inverse matrix method and hence can be accepted to be further used in the following analysis.

3.5. Contributions of different transfer paths

The contour plots of the contributions of all the 15 transfer paths to the vibration of the steering wheel along the X direction in the frequency range of 0–180 Hz are shown in Fig. 7. In the figure, the red color indicates that the contribution is of high value, and the blue color indicates that the contribution is of low value. In the figure, several vertical lines representing high vibration accelerations at the frequencies of integers multiple of the engine
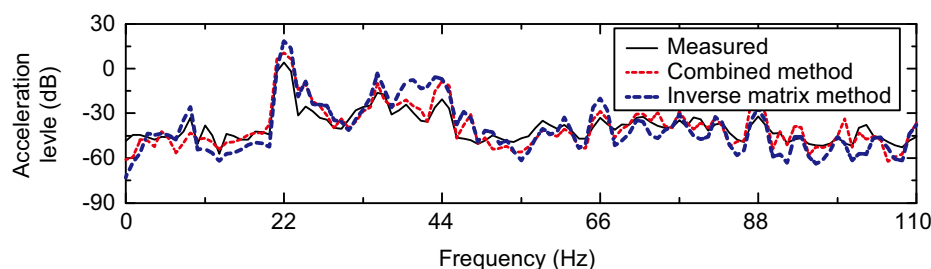

Fig. 6. Comparisons of the calculated and measured vibration accelerations of the steering wheel along the X direction.
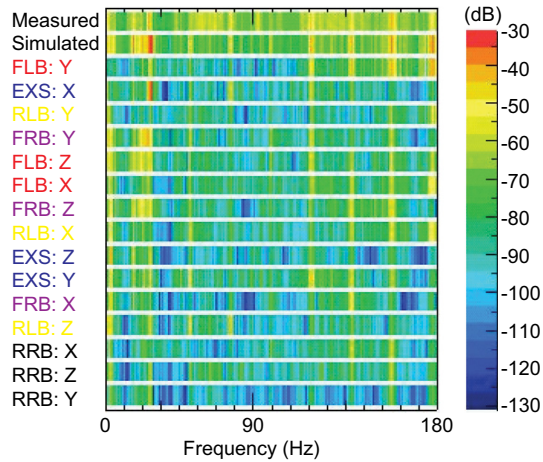
Fig. 7. Contour plots of the contributions of the transfer paths to the vibration of the steering wheel along the X direction at the frequency range of 0–180 Hz.

ignition frequency are clearly seen. Due to the fact that the vibration at the engine ignition frequency is the largest and it is the focus of this study, the contributions of the transfer paths at this frequency are further plotted in Fig. 8. The bar plots clearly show that the contribution of the vibration of the exhaust system along the X direction is the largest, and the vibration of the RLM along the Y direction has the second largest contributions to the vibration of the steering along the X direction. It seems that the vibrations of the four rubber mounts along the Z direction have larger contributions than the vibrations along the X and Y directions, and the vibrations of the four rubber mounts along the X direction are smaller than the vibration accelerations along the Y and Z directions. This result leads us to give a further observation on the operational forces and FRFs because the vibrations are the combined effects of the operational forces and FRFs.

Because the contributions of the vibrations of the exhaust system along the X and Z directions and the ones of the RLM along the Y and Z directions are among the largest, the operational forces and FRFs of the exhaust system and the RLM are to be compared. The operational forces of the exhaust system and RLM along the X, Y and Z directions are compared as shown in Figs. 9 and 10, respectively. In the figure, there are no data points in the frequencies of 0 and 1 Hz. This is because the data in the frequencies are not within the lower and upper bounds in the abscissa, and thus the data points were not presented in the figure. This type of treatment is to be performed for the other two figures (Figs. 12 and 16). The figures showed that the operational forces along the Y direc-

tion are the largest, and the operational forces along the X direction are the smallest for both of the operational forces of the exhaust system and RLM along the X, Y and Z directions at most of the frequencies. This result implied that larger contributions of the vibrations of the exhaust system along the X direction might not be caused by the operational force of the exhaust system along the X direction.

The FRFs of the transfer paths between the steering wheel along the X direction and the exhaust system and RLM along the X, Y and Z directions are compared as shown in Figs. 11 and 12, respectively. For the FRFs between the steering wheel along the X direction and the exhaust system, no obvious trends can be found in the frequency range of 0–110 Hz. For the FRFs between the steering wheel along the X direction and the RLM, the FRFs along the Y direction are the largest at most of the frequencies. However, big differences in the FRFs at some frequencies can be obviously observed. It is seen that the FRFs of the exhaust system along the Y direction are the largest at the frequencies around 4, 24 and 41 Hz, and the FRFs of the exhaust system along the X direction is the largest at the engine ignition frequency. This result indicates that the large FRFs of the exhaust system along the X direction might be the main cause of larger contribution of the exhaust system along the X direction. The peaks at the frequencies around 4, 24 and 41 Hz might also affect the comfort of steering wheel. They are not to be further analyzed because the focus of this study is the vibration at the ignition frequency of 22 Hz.

4. Structural modifications to reduce the vibration

Based on the above experimental results, it is seen that the FRFs of the exhaust system along the X direction might be the root cause of the protruded vibration of the steering wheel along the X direction at the engine ignition frequency. Therefore, the mounting structure of the exhaust system is modified in order to reduce the vibration. In order to achieve this goal, the modal analysis using finite element method was employed, which is considered to be effective in solving dynamic related engineering problems [19–21]. The modal characteristics of the original mounting structure were firstly analyzed, and then the mounting structure was modified to improve the modal characteristics. The layout of the original mounting structure is shown in Fig. 13(a), and the layout of the modified mounting structure is also presented as shown in Fig. 13(b).

For the finite element model of the mounting structure, the two-dimensional shell elements were used because the thickness of the mounting structure was quite small. The element size was 10 mm, and nodular cast iron (Q235) was used. the material properties for nodular cast iron including the elastic modulus, Poisson
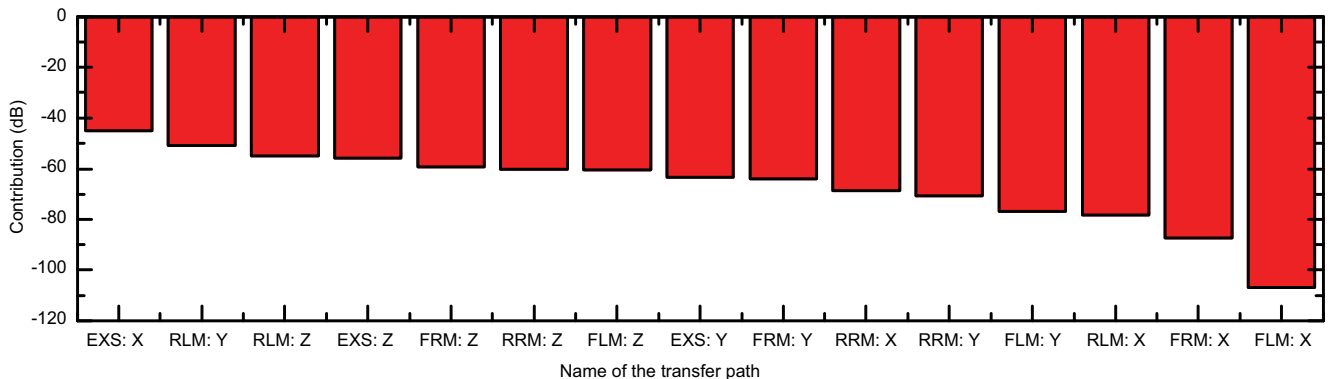

Fig. 8. Bar plots of the contributions of the transfer paths to the vibration of the steering wheel along the X direction at the engine ignition frequency of 22 Hz.
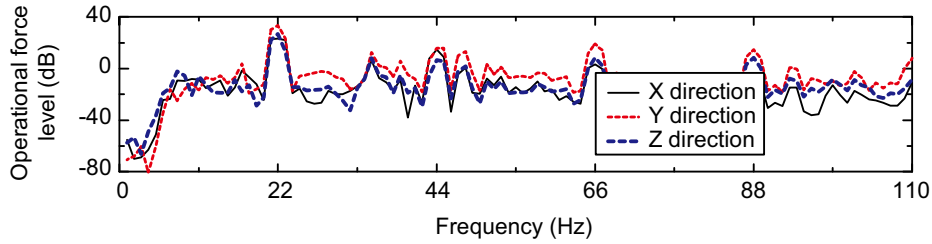
Fig. 9. Comparisons of the simulated operational forces of the exhaust system along the X, Y and Z directions.
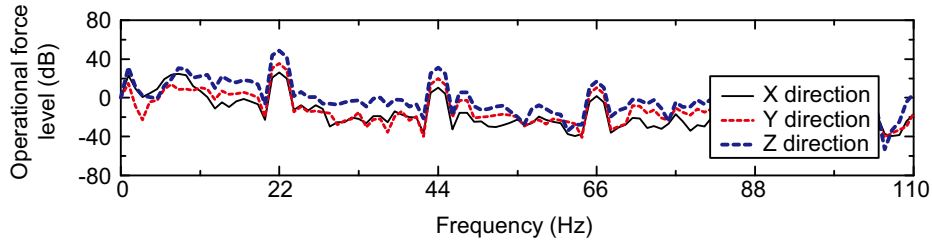

Fig. 10. Comparisons of the simulated operational forces of the RLM along the X, Y and Z directions.
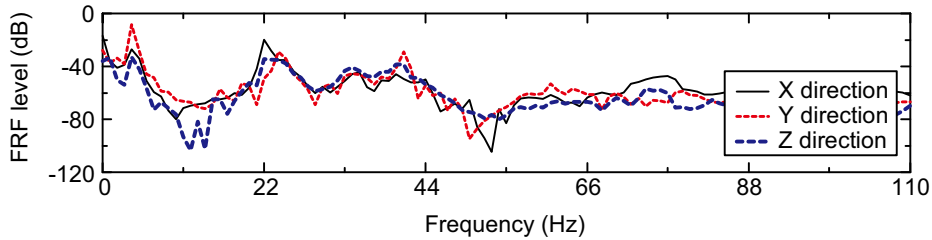

Fig. 11. Comparisons of the FRFs of the transfer paths between the steering wheel along the X direction and the exhaust system along the X, Y and Z directions.
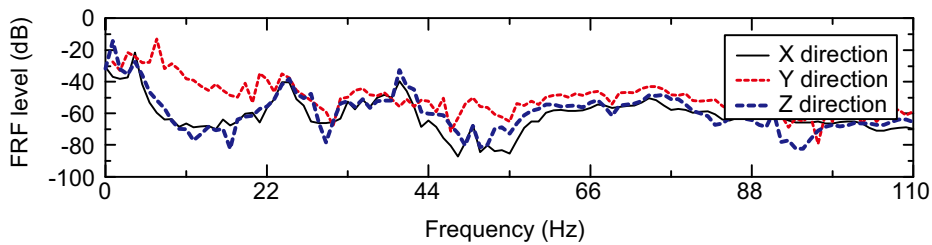

Fig. 12. Comparisons of the FRFs of the transfer paths between the steering wheel along the X direction and the RLM along the X, Y and Z directions.
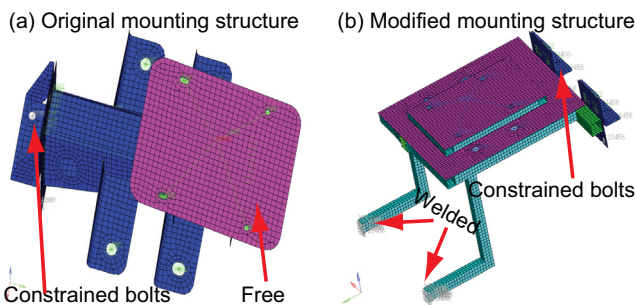

Fig. 13. Layouts of the original and modified mounting structures of the exhaust system.

ratio and density were 210 GPa, 0.28 and 7850 kg/m³, respectively. In order to reflect the actual mounting condition, the three translational degree of freedoms of the four mounting holes were constrained. The Lanczos method was used to calculate the modal characteristics. The first six mode shapes of the original mounting structure are shown in Fig. 14. The first two mode shapes at the natural frequencies of 93 Hz and 117 Hz are of the global mode shapes, vibrating along the global Z and X directions, respectively. The third to sixth mode shapes at the natural frequencies of 124 Hz, 132 Hz, 134 Hz and 230 Hz are mainly the local mode shapes located in the mounting plate of the air filter. The deformations of the mounting plate of the air filter are quite large for the third to six modes. This is mainly caused by the cantilever
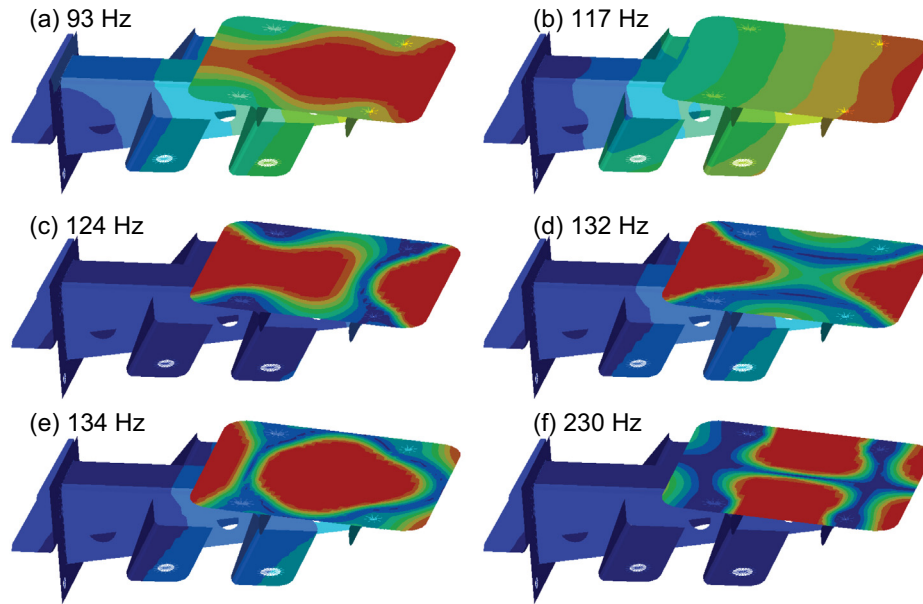
Fig. 14. Simulated first six mode shapes of the original mounting structure of the exhaust system.

mounting type of the original mounting structure, resulting in large distance between the mounting plate of the air filter and the constrained bolts.

Therefore, the mounting structure of the exhaust system was modified to avoid the cantilever mounting type. This is achieved by performing the following modifications to the mounting structure as shown in Fig. 13(b). The silencer was mounted on the plane constructed by seven square steels, four square steels (type $20 \times 20 \times 260$ mm and $20 \times 20 \times 320$ mm) were used to connect the mounting plates of the air filer and the silencer by welding. Two L-like square steels were used to connect the mounting structure with the surrounding mounts by welding. In addition, two more mounting structures were designed to make the mounting structure more stable, and the mounting structure and the body frame of the passenger vehicle were tightly assembled. The mode shapes of the modified mounting structure of the exhaust system are shown in Fig. 15. It is clearly seen that the natural frequencies are improved significantly, the six mode shapes are mainly of the local mode shapes, and the deformations of the mounting structure are decreased. These results implied that the modal characteristics of the modified mounting structure of the exhaust system are improved.

In order to further verify the effectiveness of the proposed mounting structure, the vibrations of the steering wheel using the modified mounting structure were measured. A comparison of the measured vibrations of the steering wheel along the X, Y and Z directions are shown in Fig. 16. The figure shows that the vibrations are obviously reduced at most of the frequencies when the modified mounting structure was used. Specially, the vibration accelerations of the steering wheel along the X and Y directions are reduced from 5.296 dB and −5.780 dB to −0.094 dB and −11.109 dB at the engine ignition frequency, whereas the vibration accelerations along the Z direction increases slightly (from −11.294 dB to −8.115 dB). Due to the fact that the vibration accelerations along the X and Y directions are larger than that along the Z direction at the engine ignition condition, the vibrations of the steering wheel are hence reduced. These results indicated that the vibrations of the steering wheel can be improved by the modified mounting structure, which validates the effectiveness of the proposed mounting structure.
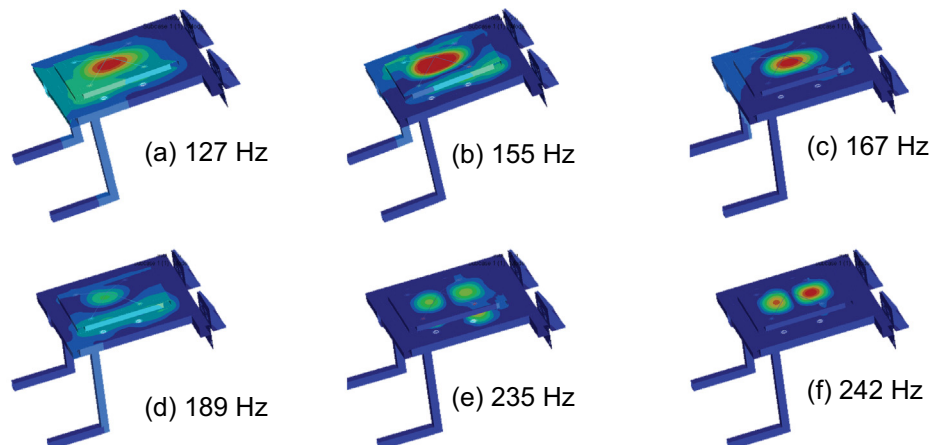

Fig. 15. Simulated first six mode shapes of the modified mounting structure of the exhaust system.
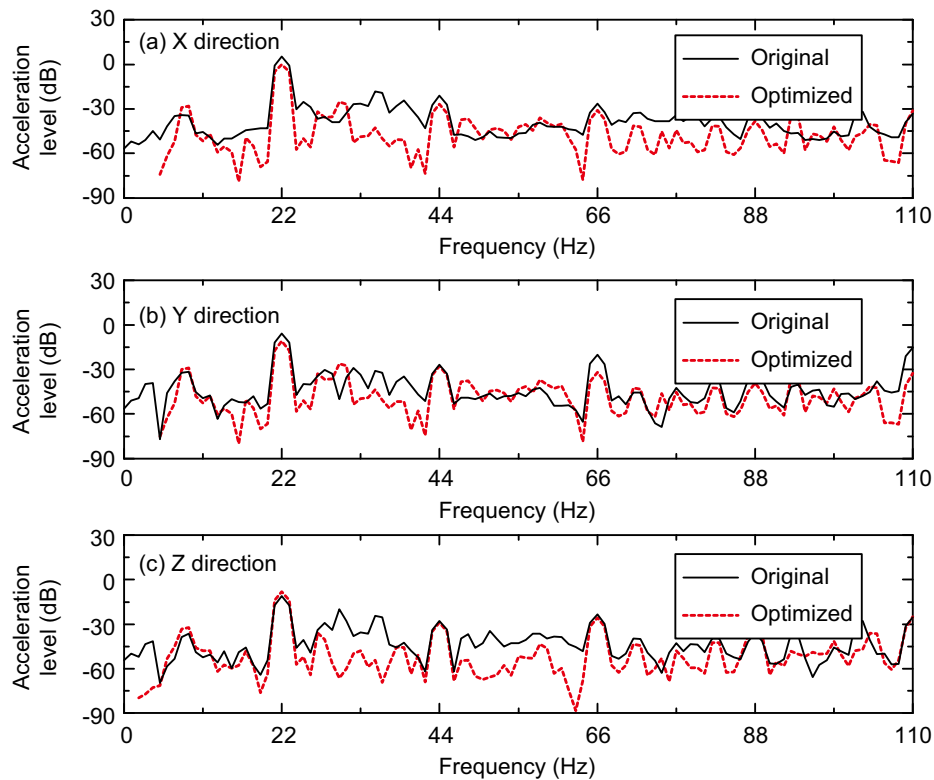
Fig. 16. Comparisons of the vibration accelerations of the steering wheel along the X, Y and Z directions using the original and modified mounting structures.

5. Conclusions

A systematic analysis methodology has been proposed to analyze and reduce the low-frequency vibration of steering wheel using classical transfer path analysis (CTPA). The result in the vibration measurement of the steering wheel demonstrated that the vibration accelerations of the steering wheel at the engine ignition frequency of 22 Hz are protruded, and the vibration acceleration along the X direction is the largest, far larger than the vibration accelerations along the Y and Z directions.

By analyzing and comparing the contributions of different transfer paths to the vibration of steering wheel, the operational forces in the four rubber mounts and exhaust systems, and the frequency response functions (FRFs) between the four rubber mounts and exhaust systems and the steering wheel, the main causes leading to the vibration of steering wheel are identified. The results revealed that the vibration of the exhaust system along the X direction contributes most to the vibration of steering wheel along the X direction because of large FRF.

According to the above findings, the mounting structure of the exhaust system has been modified based on modal analysis results. The modified mounting structure has better modal characteristics than the original mounting structure in both the mode shapes and modal frequencies. A comparison of the vibrations of steering wheel using the original and modified mounting structures has shown that the dominant vibrations of the steering wheel can be significantly reduced. The proposed analysis methodology and structural modification method is efficient in the development of more comfortable passenger vehicles.

Acknowledgement

Appendix A. Supplementary material

Supplementary data to this article can be found online at https://doi.org/10.1016/j.apacoust.2019.107021.

References

[1] Wang J, Chang S, Liu G, et al. Optimal rib layout design for noise reduction based on topology optimization and acoustic contribution analysis. Struct Multidiscip Optim 2017:1–16.
[2] Huang HB, Huang XR, Wu JH, et al. Novel method for identifying and diagnosing electric vehicle shock absorber squeak noise based on a dnn. Mech Syst Signal Process 2019;124:439–58.
[3] Dai WQ, Zheng X, Luo L, et al. Prediction of high-speed train full-spectrum interior noise using statistical vibration and acoustic energy flow. Appl Acoust 2019;145:205–19.
[4] Zheng X, Dai W, Qiu Y, et al. Prediction and energy contribution analysis of interior noise in a high-speed train based on modified energy finite element analysis. Mech Syst Signal Process 2019;126:439–57.
[5] Zhang JH, Xia SQ, Ye SG, et al. Experimental investigation on the noise reduction of an axial piston pump using free-layer damping material treatment. Appl Acoust 2018;139:1–7.
[6] Ye SG, Zhang JH, Xu B, et al. Experimental studies of the vibro-acoustic characteristics of an axial piston pump under run-up and steady-state operating conditions. Measurement 2019;133:522–31.
[7] Zhang JH, Xia SQ, Ye SG, et al. Sound quality evaluation and prediction for the emitted noise of axial piston pumps. Appl Acoust 2019;145:27–40.
[8] Ye S, Zhang J, Xu B, et al. Theoretical investigation of the contributions of the excitation forces to the vibration of an axial piston pump. Mech Syst Signal Process 2019;129:201–17.
[9] Du H, Zhang QM, Chen SM, et al. Modeling, simulation, and experimental validation of electro-hydraulic power steering system in multi-axle vehicles. Proc Inst Mech Eng Part D – J Automobile Eng 2019;233(2):317–32.

[10] De Klerk D, Rixen DJ. Component transfer path analysis method with compensation for test bench dynamics. Mech Syst Signal Process 2010;24 (6):1693–710.

[11] De Sitter G, Devriendt C, Guillaume P, et al. Operational transfer path analysis. Mech Syst Signal Process 2010;24(2):416–31.

[12] Janssens K, Gajdatsy P, Gielen L, et al. Opax: a new transfer path analysis method based on parametric load models. Mech Syst Signal Process 2011;25 (4):1321–38.

[13] Wang Z, Zhu P, Zhao J. Response prediction techniques and case studies of a path blocking system based on global transmissibility direct transmissibility method. J Sound Vib 2017;388:363–88.

[14] Moorhouse AT, Elliott AS, Evans TA. In situ measurement of the blocked force of structure-borne sound sources. J Sound Vib 2009;325(4):679–85.

[15] Elliott AS, Moorhouse AT, Huntley T, et al. In-situ source path contribution analysis of structure borne road noise. J Sound Vib 2013; 332(24):6276–95.

[16] Lennström D, Olsson M, Wullens F, et al. Validation of the blocked force method for various boundary conditions for automotive source characterization. Appl Acoust 2016;102:108–19.

[17] Diez-Ibarbia A, Battarra M, Palenzuela J, et al. Comparison between transfer path analysis methods on an electric vehicle. Appl Acoust 2017;118(Suppl. C):83–101.

[18] Shin T, Kim YS, An K, et al. Transfer path analysis of rumbling noise in a passenger car based on in-situ blocked force measurement. Appl Acoust 2019;149:1–14.

[19] Xiang JW, Lei YG, Wang YX, et al. Structural dynamical monitoring and fault diagnosis. Shock Vib 2015:3.

[20] Xiang JW, Yang ZB, Aguilar JL. Structural health monitoring for mechanical structures using multi-sensor data. Int J Distrib Sens Netw 2018;14(9):3.

[21] Wang S, Xiang J, Tang H, et al. Minimum entropy deconvolution based on simulation-determined band pass filter to detect faults in axial piston pump bearings. ISA Trans 2019;88:186–98.